1

Semiconductor Quantum Dots

This thesis deals with electron tunneling between semiconductor nanocrystals (quantum dots) and a metal. In this chapter, we discuss the confinement of the electron wave functions in a nanocrystal (size quantisation) and the basic principles of electron tunneling. The importance of surface atoms and the corresponding surface electron levels for the optical and electronic properties of quantum dots is discussed. To study their (opto)electronic properties we have attached the quantum dots to a conducting substrate. A metal electrode with a monolayer of semiconductor quantum dots has been investigated in a photoelectrochemical cell. Photoinduced electron tunneling between the nanocrystals and the metal electrode or a redox system in the electrolyte was investigated by a time-resolved photoelectrochemical technique (Intensity-Modulated Photocurrent Spectroscopy). Alternatively, the electronic properties of individual quantum dots were studied by Scanning Tunneling Spectroscopy. The principle of these two techniques is described.

1.1 Introduction

A crystalline material which is size-restricted in three dimensions such that the electron wave functions are confined within its volume is called a quantum dot (QD). Due to this confinement the electronic properties of quantum dots depend on their size in the nanometer regime.[1,2] This effect, now called 'size-quantisation', was first observed in 1926 with CdS colloids[3], but was only properly recognized in the 1980's.[4,5] Chemists and physicists have studied nanostructures extensively in the past two decades in order to understand the size-quantisation effects in semiconducting and metal quantum dots.

Due to their extremely small sizes and their interesting electronic properties, quantum dots are promising building blocks for the fabrication of electronic and optoelectronic solid state devices. Integrated circuits (ICs) might be further miniaturised by using nanocrystallites. The II–VI nanocrystals have a bandgap which can be tuned in a broad range (up to 4 eV) by changing either their size or chemical composition; this makes them suitable candidates for applications as a Light Emitting Diode (LED)[6,7], a Single Electron Transistor (SET)[8-10], chromophores in solar cells[11-15], or as a 'building block' for photonic crystals.[16] Recently, a LED with an efficiency of 10 %, based on CdSe nanocrystals in a semiconducting polymer matrix, was fabricated.[17,18] The output colour could be tuned in the entire visible range. A critical parameter for the performance of a SET, the principle of which is based on the Coulomb blockade effect, is the capacitance of the quantum dot, which is determined by its size. Quantum dots can be applied as stable fluorescent indicators in biological research; core-shell quantum structures of CdSe/ZnS have a very high luminescence quantum yield (up to100%). Since they can easily be attached to DNA[19] or proteins by a sulphide bond they can act as a luminescing label to monitor biological reactions. Semiconductor colloids can also be employed in photocatalysis; TiO_2 colloids irradiated with UV-light can photo-oxidize organic contaminants.[20]

Methods for the preparation of large quantities of well-defined nanoparticles have been developed in order to study the size-quantisation effect. A technique to grow low-dimensional structures, Molecular Beam Epitaxy (MBE), was developed at the end of the 1960's.[22,23] Arrays of quantum dots on substrates can be prepared by MBE or lithographic dry-etching.[24-25] Alternatively, quantum dots can be formed in the gas phase by laser vaporisation[25] or as colloids in suspension.[27,28] Chemists have succeeded in greatly improving the monodispersity in size and shape of colloidal semiconductor quantum dots in the past decade.[29] High-quality suspensions can now be synthesised and the size distribution can be further narrowed by size-selective precipitation or photoetching.[30-32]

Optical absorption and photoluminescence were first used to study the electronic structure of nanometer-sized semiconductor colloids. However, these techniques only provide information about the collective properties of large numbers of QDs and, due to a distribution in particle size, the luminescence signals are inhomogeneously broadened. With Scanning Probe Techniques such as Scanning Tunneling Spectroscopy (STM) and Scanning Near-field Optical Microscopy (SNOM), electrical and optical measurements on individual particles can be performed, avoiding problems arising from polydispersity.

In the work described in this thesis the optoelectronic properties of semiconductor quantum dots, and charge transfer between such structures and a conducting substrate were studied in a novel way. For this purpose, metal substrates were provided with a (sub)monolayer of quantum dots; the optoelectrical properties of the systems were investigated with time-resolved photoelectrochemistry. The electronic structure of individual nanocrystals was investigated by Scanning Tunneling Spectroscopy at room temperature and at 4 K. This chapter presents an introduction to the size-quantisation effect in semiconductors and electron transfer between a metal and a semiconductor quantum dot. In the latter sections the principles of the measuring techniques are explained and an outline of this thesis is given.

1.2 Size-quantisation in Semiconducting Nanocrystals

1.2.1 Energy Bands in Bulk Semiconductor Crystals

To discuss the origin of energy bands in bulk semiconductors and electron tunneling between two systems, a single electron in a crystal is considered.[33] The time-independent Schrödinger equation for an electron can be written as,

$$-\frac{\hbar^2}{2m_e}\nabla^2\,\Psi(x,y,z)+U(x,y,z)\,\Psi(x,y,z)=E\,\Psi(x,y,z) \qquad (1.1)$$

where m_e is the mass of the free electron, E is the kinetic energy, and $\nabla^2=\left(\frac{\partial^2}{\partial x^2}+\frac{\partial^2}{\partial y^2}+\frac{\partial^2}{\partial z^2}\right)$. In the free-electron approach, the potential energy of the electron due to the crystal lattice of core ions *U(x,y,z)* is neglected, and is taken as a constant (e.g. *U(x,y,z)* =0). In that case the solution of equation (1.1) for $\Psi(x,y,z)$ can be denoted as,

$$\Psi_{\vec{k}}(\vec{r}) = \frac{1}{\sqrt{V}} e^{i\vec{k}\cdot\vec{r}} \tag{1.2}$$

where $\vec{r}$ is the position vector (x,y,z), and $\vec{k}$ is the wave-vector $\left(k_x,k_y,k_z\right)$; the plane periodic wave, $e^{i\vec{k}\cdot\vec{r}}$, has a constant amplitude in any plane perpendicular to $\vec{k}$, and is periodic along lines parallel to $\vec{k}$, with a wavelength $\lambda_e = \frac{2\pi}{k}$. The prefactor $\frac{1}{\sqrt{V}}$ is due to the normalisation condition, which requires that the particle must be present in the sample volume V. The linear momentum of the electrons is $\vec{p} = \hbar\vec{k}$ and the kinetic energy is given by,

$$E\left(\vec{k}\right) = \frac{\hbar^2 k^2}{2m_e} \tag{1.3}$$

The occupation of the electron levels is in accordance with the Pauli exclusion principle. At 0 K, all energy levels below the Fermi-energy (E_F) are occupied by two electrons of opposite spin. The occupation of electron energy levels under thermal equilibrium at T > 0 K can be derived from statistical thermodynamics. The probability that an energy level, E, is occupied by an electron is given by the Fermi-Dirac function,

$$f(E) = \frac{1}{1+e^{(E-\mu_e)/k_BT}} \tag{1.4}$$

in which μ_e is the electrochemical potential (Fermi-level) and k_B the Boltzmann constant. The free electron model can be refined by taking the scattering of the electron waves by the periodic lattice potential energy *U(x,y,z)* into account. The distance between the centres of the core ions in the x-direction is denoted as d_x. The electrons with low energy have wavelengths much longer than d_x; however, at higher energy there are free electrons with wavelengths obeying the condition for Bragg reflection,

$$\frac{\lambda_e}{2} \cong \frac{d_x}{q} \qquad (q=\pm1, \pm2, ..) \tag{1.5}$$

Due to Bragg scattering on the periodic lattice potential, propagation of these electrons will be prohibited in the x-direction and standing waves are formed. Two standing waves can be constructed by a linear combination of the waves travelling in the positive and negative

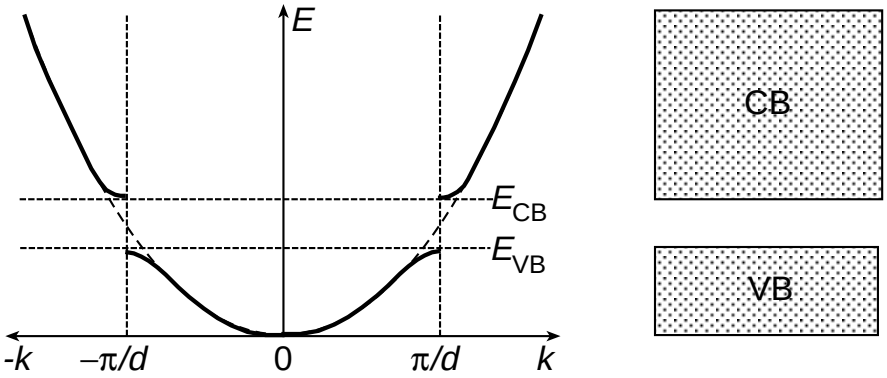

Figure 1.1 *The formation of energy bands in a macroscopic semiconductor due to Bragg reflection of the electrons on the periodic lattice of the crystal.*

x–directions. The electron density corresponding to the first standing wave is centered at the core ions, that of the second wave between the core ions. The two standing waves correspond to considerably different energies. The energy difference can be estimated by a perturbation method; it is equal to the periodic lattice potential in the x-direction. The scattering of the free electrons by the periodic lattice leads to discontinuities in the *E(k)* relationship for *k* values at around $k = q\frac{\pi}{d}$. These discontinuities lead to the formation of energy bands, separated by energy gaps, as presented in Figure 1.1. This derivation for the x-direction can be used in a similar way for the y and z-directions. The *E(k)* relationship for free electrons is a good approximation for most of the electrons in a band, except for those near the edge of the Brillouin zones.

1.2.2 Quantum Size Effects

A (Wannier) exciton can be defined as the bound state of an electron-hole pair, which is due to a Coulomb interaction between the charge carriers.[1] The distance between the electron and the hole is the Bohr radius of the exciton, a_B, and is given by,

$$a_B = \frac{4\pi\varepsilon_0\varepsilon_\infty \hbar^2}{m_0 e^2}\left(\frac{1}{m_e^*} + \frac{1}{m_h^*}\right) \tag{1.6}$$

in which m_e^* and m_h^* are the effective electron and hole masses, respectively, and ε_∞ is the high-frequency relative dielectric constant of the medium. The resulting Bohr radius is much larger than that of a hydrogen atom, since the effective masses are considerably smaller than the mass of

the electron at rest, m_0, and ε_∞ is considerably larger than 1. Values for a_B for the common semiconductors are in the range 10-100 Å.

Nanocrystals have crystalline order and dimensions corresponding to some tens of a lattice constant in each direction. Electron scattering with the lattice leads to band formation, as for macroscopic crystals. However, the free electron wavelength and the Bohr radius can be comparable to or even larger than the crystal dimensions. This means that the nanocrystal acts as a quantum box for quasiparticles. The symmetry of the box is important for the solution of the Schrödinger equation. In the literature, a spherical symmetry is often used. For simplicity, we consider a rectangular box of dimensions L_x, L_y, and L_z surrounded by infinitely high energy walls. Stable solutions of the Schrödinger equation are standing waves. For instance in the x-direction, the free-electron and free-hole standing waves must fulfill,

$$L_x = n_e \times \frac{\lambda_e}{2} \qquad (n_e = \pm 1, \pm 2, ...) \tag{1.7}$$

$$L_x = n_h \times \frac{\lambda_h}{2} \qquad (n_h = \pm 1, \pm 2, ...) \tag{1.8}$$

From equations (1.5), (1.7) and (1.8) it follows that size quantisation in the x-direction gives discrete k_x values for the electrons and holes. The total number of discrete states depends on the well width and depth. In the case of walls with a finite height, the wave function does not vanish at the edge of the well, but decays exponentionally in the classically forbidden region. Therefore, the probability of finding a particle inside the well is always less than unity and decreases with increasing E_n. As a result of the reduced number of states and the confinement of the electron wave functions, a part of the *E(k)* curve is replaced by discrete points as shown in Figure 1.2. We return to this model in chapter 6.

Brus has modelled electron confinement in a spherical box by using the effective mass approximation[5,34] When $R << a_B$ the confined electron and hole have no bound state as in the definition of an exciton given above and the Coulomb interaction may be ignored to a first approximation. The mathematical treatment is similar to that for an electron in the spherical potential well of a nucleus.[35] The state of the system is characterized by three quantum numbers, namely the principal number *n*, the orbital number *l*, and the magnetic number *m*. The states corresponding to different *l* values are denoted as *s*-, *p*-, *d*-, and *f*- states. Each state with a given *l* value has a $(2l+1)$ degeneracy, corresponding to $m = 0, \pm 1, \pm l$. For a spherically symmetrical potential box with an infinite barrier, the resulting energy of the exciton can be written as follows,

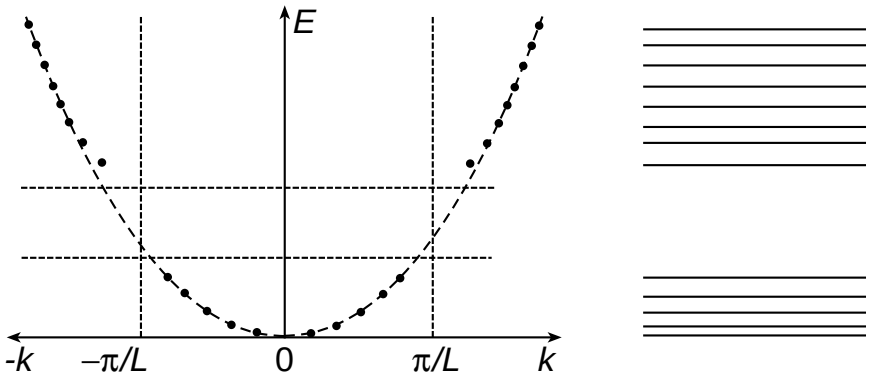

Figure 1.2 *Due to the size-confinement of the semiconductor nanocrystal only the electron wave functions obeying R=nλ/2 can form standing waves; this and the reduced number of states lead to the formation of discrete energy levels instead of energy bands.*

$$E_{nl} = E_g + \frac{\hbar^2 \chi_{nl}^2}{2m_0 R^2}\left(\frac{1}{m_e^*} + \frac{1}{m_h^*}\right) \tag{1.9}$$

in which E_g is the bandgap of the macrocrystalline semiconductor, defined as the energy needed to excite an electron from the top of the valance band to the bottom of the conduction band. χ_{nl} is the n^{th} root of the spherical Bessel function and l the order of the function; for l=0 (so-called *s*-states) $\chi_{n0}=\pi n$.

Weakly quantised quantum dots (with $R \sim a_B$) contain a large number of atoms and unit cells; therefore Bragg reflection at the periodic lattice will lead to the formation of continuous energy bands. Only the levels at the top of the valence band and at the bottom of the conduction band, which correspond to the most delocalised electron wave function, will be discrete (see Figure 1.3 (b). Highly quantised semiconductor quantum dots are sometimes called artificial atoms because they exhibit a discrete optical spectrum determined by their size (see Figure 1.3 (c)).

The electron and hole, confined in a space with dimensions smaller than the Bohr radius of the exciton, cannot however be considered as independent particles; the Hamiltonian must be expanded by two-particle kinetic terms and the Coulomb and confinement potential. This leads in the Brus model to an expression for the energy of the ground state of the electron-hole pair ($1s_e1s_h$ or first excited state),

$$E(1s_e 1s_h) = E_g + \frac{\pi^2 \hbar^2}{2 m_0 R^2}\left(\frac{1}{m_e^*} + \frac{1}{m_h^*}\right) - A\frac{e^2}{4\pi\varepsilon_0\varepsilon_\infty R} \tag{1.10}$$

in which the second term describes confinement and the third the Coulomb electron-hole interaction. The coefficient *A* corresponds to 1.786 for the $1s_e1s_h$ state and has values between 1.6 and 1.9 for other states.[36] Equation (1.10) implies that the gap between the filled valence band levels and the empty conduction band levels increases when the radius of the particle decreases. Due to the electron-hole Coulomb interaction, the measured optical bandgap has a slightly lower energy than the 'actual' electronic band gap.

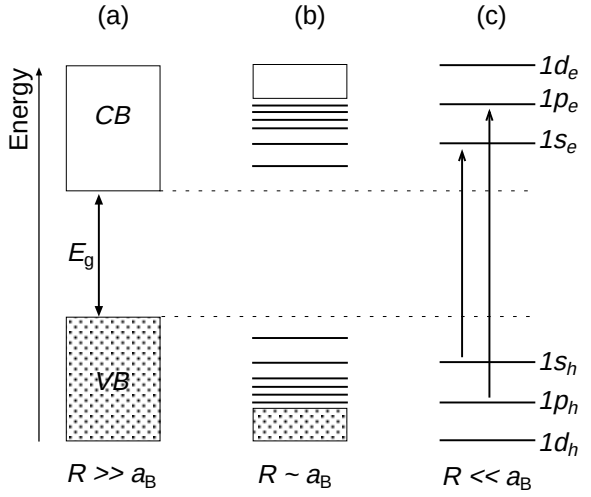

Figure 1.3 *The effect of size on the electronic structure of a semiconductor crystal for three different size-ranges. (a) a macrocrystalline semiconductor ($R>>a_B$) with continuous energy bands; the filled valence band (VB) and empty conduction band (CB) and the bandgap energy (E_g) are shown. (b) semiconductor nanocrystal with a weak size-quantization ($R\sim a_B$). (c) highly quantised dot ($R<<a_B$) with discrete atomic-like energy levels and optical transitions.*

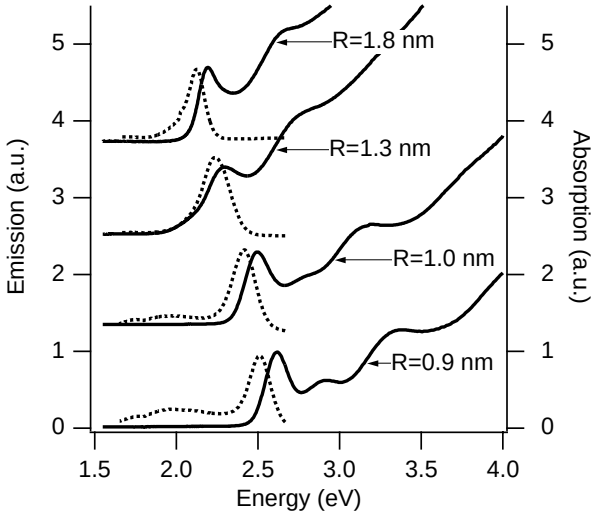

Figure 1.4 *Absorption (solid lines) and emission (dotted lines) spectra of colloidal CdSe quantum dots, showing that the absorption edge shifts towards higher energies with respect to bulk CdSe (1.84 eV) and that discrete energy bands become more pronounced as the particle size decreases.*

The increase of the bandgap and the transition from continuous energy bands to discrete energy levels upon a decrease of particle size has been observed by optical absorption spectroscopy in many colloidal semiconductor systems.[30,37] The absorption and emission spectra of colloidal CdSe quantum dots of different sizes studied in this work (see Figure 1.4) demonstrate these effects. Upon a decrease of the particle radius, the onset of the absorption and the emission maximum shift towards higher energies. A clear structure in the absorption spectra is observed for the smallest particles, corresponding to discrete optical transitions.

1.2.3 Surface States

Although the presence of surface states is by no means a size-quantisation effect, surface states become increasingly important as the size of a structure reduces; the ratio of the number of surface to bulk atoms, which increases with decreasing particle radius, is very large for quantum dots. Surface atoms give rise to electron levels of energy different from those of the bulk levels; these levels can play an important role in light absorption and emission.[38] The importance of surface states in the photoexcited decay dynamics has become clear from time-resolved luminescence spectroscopy on colloidal suspensions of quantised PbS, CdS, CdSe, ZnO, and InP.[39-42] Besides direct conduction-to-valence band recombination, a broad band at lower energy is often observed in emission spectra;[37] this sub-bandgap emission can correspond to a transition either from the conduction band to a bandgap state, or from a bandgap state to the valence band. Alternatively, surface states can provide pathways for non-radiative recombination and therefore decrease the luminescence quantum yield. Charge carriers can also be trapped in deep bandgap states, forming a long-lived excited state of lower energy.[43]

1.3 Electron Tunneling

1.3.1 Basic Principles of Electron Tunneling

Metals and semiconductors generally have a high potential energy barrier at their surface, which confines the electrons within the solid.[44] At room temperature thermally activated escape of the electrons over the surface barrier is very improbable. However, quantum mechanical tunneling can occur when the interfacial barrier is very thin. This is the main mechanism of electron transfer through an insulating barrier between two solids in intimate contact.

The free electron model discussed in section 1.2 allows a more quantitative discussion of the probability of finding an electron in a limited region just outside a crystal. The potential energy in the crystal is set to zero, and that of an electron at rest outside the crystal to E_{vac}. The Fermi-energy of the electrons in the crystal is considerably below E_{vac}; The work function, $E_{vac}-\mu_e$, is generally of the order of a few eV. The Schrödinger equation for a single free electron in the region outside the crystal for the x-direction is given by,

$$-\frac{\hbar^2}{2m_e}\frac{\partial^2}{\partial x^2}\Psi(x)+E_{vac}\ \Psi(x)=E\ (x)\Psi(x) \tag{1.11}$$

The energy of the electron at rest in vacuum is larger than the total energy *E(x)* of the impinging electron. A solution of equation (1.11) is,

$$\Psi_{vac}(x)=\frac{1}{\sqrt{L}}e^{-\kappa_{vac}\,x} \tag{1.12}$$

where *x* is the distance from the surface and κ_{vac} the decay parameter in the x-direction

$$\kappa_{vac}=\left[\frac{2m_e\left(E_{vac}-E(x)\right)}{\hbar^2}\right]^{\frac{1}{2}} \tag{1.13}$$

The wave function of an electron impinging on a surface wall decays exponentially outside the metal. The decay length $1/\kappa_{vac}$ depends on the effective barrier height E_{vac}-*E(x)*. Tunneling of an electron between two solid phases can occur if these phases are separated by a distance of the order of $1/\kappa_{vac}$. The probability of tunneling is relatively small when $x>1/\kappa_{vac}$ (strong attenuation), and is then given by,

$$T=T_0e^{-2\kappa_{vac}\,d} \tag{1.14}$$

The distance dependence of the tunneling probability is determined by the exponential term, since the prefactor depends only weakly on the effective barrier height. Electrons close to the Fermi-energy which fulfill the condition $k_x^2 >> k_y^2+k_z^2$ have the highest tunnel probability for a barrier width, *d*. The rate constant for electron tunneling, *i.e*. the number of tunneling events per electron level per second, can be defined as,

$$k = k_0 e^{-\beta d} \tag{1.15}$$

in which k_0 is the maximum number per second for $d \rightarrow 0$, and β is equal to $2\kappa_{vac}$. A typical value of β for an effective barrier height of 1 eV is 1.0 Å^{-1}. A change of 1 Å in the barrier width typically leads to a change of the tunneling rate by a factor 2.71. This extreme sensitivity of the tunneling rate to the barrier width forms the basis for the Scanning Tunneling Microscope (STM), developed in 1982.[45] Already in 1922 field emission from metals was observed[46] and since 1937 the Field-Emission Microscope (FEM) has been used to study electron tunneling and the surface structure of metals.[47] Since 1960 electron tunneling was studied with planar metal/insulator(vacuum)/metal junctions.[48,49]

1.3.2 Electron Tunneling between a Quantum Dot and a Metal

Colloidal semiconductor quantum dots can be adsorbed on a metal electrode by Van der Waals interactions of the capping molecules, which stabilize the dots in the suspension, with the metal surface. Alternatively, covalent anchoring of the dots to the metal is possible with a difunctionalised Self-Assembled Monolayer (SAM).[50-55] In addition, QDs can be grown electrochemically on a conductive substrate; the particle size can be controlled by the charge used to electrodeposit the dots.[56-58]

A metal coated with a (sub)monolayer of nanocrystals can be used as working electrode in a conventional electrochemical cell. With such electrodes we have performed time-resolved photoelectrochemistry. The metal electrode, coated with a monolayer of dots, can be considered as a 2D array of mutually independent Double-Barrier Tunnel Junctions (DBTJ). The junctions are formed between the metal substrate and the dot and between the dot and the electrolyte. Using a modulated light intensity it is possible to measure the rate of photoinduced tunneling between the dots and the metal or the electrolyte solution.

With Scanning Probe techniques it is possible to perform electrical measurements on individual quantum dots. When the STM tip is positioned above a dot a DBTJ is formed consisting of the metal/dot and dot/tip junctions.[64-67] A schematic illustration of the Double-Barrier Tunnel Junction is shown in Figure 1.5 (a) for an electrical and (b) for an electrochemical configuration, and in (c) the electrical circuit of the DBTJ for both configurations is shown. The electronic properties of individual semiconductor (and metal) particles have been investigated in this way with Tunneling Spectroscopy (TS).

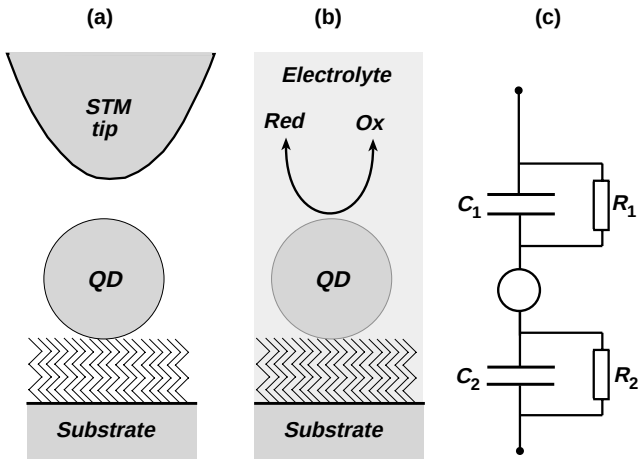

Figure 1.5 *Schematic representation of a quantum dot on a Self-Assembled Monolayer on a metal substrate in (a) an electrical setup, with the STM tip as second electrode, and (b) in an electrochemical configuration, in which the electrolyte establishes the contact with the counter electrode. In (c) the electrical equivalent circuit of the Double-Barrier Tunnel Junction is shown for the two configurations.*

1.3.3 Photoelectrochemical Measurements

The processes involved in photoinduced electron tunneling between a quantum dot and a metal electrode, forming the basis of the photoelectrochemical and electrical measuring techniques, are presented in this and the following section.

Figure 1.6 shows a quantum dot on a metal electrode. An electron has been excited from a valence band level (HOMO) to a conduction band level (LUMO) of the quantum dot upon absorption of a photon ($h\nu > E_g$). Direct band-band recombination is usually very fast (~ps) and returns the system to the ground state. However, trapping of the hole or the electron in a bandgap state may compete with the fast relaxation to the ground state. As a result, an excited state of lower energy is formed. It will become clear in this work that such a photoexcited state can possess a long lifetime, so that photoinduced tunneling between the dot and the metal can occur. Resonant tunneling of the photoexcited electron to the metal is only possible when the substrate Fermi level ($E_{F,sub}$) is below the electron level (E_e), and an electron can only tunnel from the metal to the unoccupied level in the dot when the metal Fermi level is above this level (E_h). Thus, relaxation of the excited state to the ground state via photoinduced tunneling to and from the metal can only occur when $E_h < E_{F,sub} < E_e$. Decay of the photoexcited state via the metal can be observed by time-resolved measurement of the current in the external electrical circuit. When $E_{F,sub}$ is scanned and the photoinduced tunneling currents are measured in the external circuit, the electronic levels of the long-lived excited state can be resolved. The rate constants of these

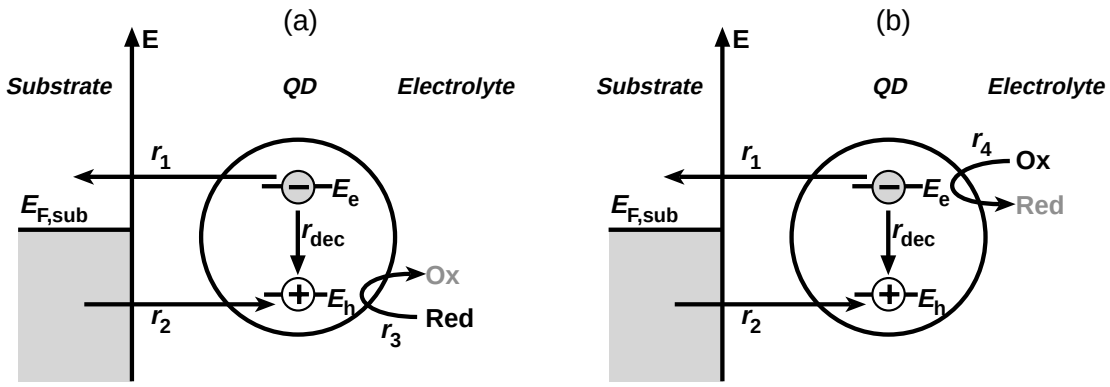

Figure 1.6 *A photoexcited quantum dot adsorbed on a metal electrode, forming a DBTJ. After a photon is absorbed, one of the charge carriers is trapped in a localised state. (a) A hole scavenger is added to the electrolyte; when r_1 is followed by r_3 a steady-state anodic photocurrent is observed. (b) An electron scavenger is added; when r_2 is followed by r_4 a steady-state cathodic photocurrent is measured.*

tunneling processes may be determined by using time-resolved photoelectrochemistry. This technique will be explained in section 1.4. In the presence of either a reducing agent (Figure 1.6(a)) or an oxidizing agent (Figure 1.6(b)), electron transfer may also occur between the dot and the electrolyte. When r_1 is followed by r_3, a steady-state anodic photocurrent will be observed. Otherwise, when r_2 is followed by r_4, a steady-state cathodic photocurrent results.

1.3.4 Electrical Measurements with a Substrate/Dot/Tip Configuration

Figure 1.7 shows an energy level scheme for a highly quantised semiconductor quantum dot (with discrete energy levels) in contact with a metal substrate. By positioning the STM tip above the particle a DBTJ is formed. For simplicity, we assume that $E_{F,sub}$ is fixed with respect to the energy levels in the quantum dot. At small bias ($\Delta E << E_g$) the Fermi levels of the tip and the substrate are located in the bandgap of the nanocrystal and resonant electron tunneling via energy levels of the dot cannot occur. If a bias potential is applied such that $E_{F,tip}>E_{F,sub,}$ resonant tunneling of an electron from the tip to the dot and from the dot to the substrate can occur when $E_{F,tip}$ reaches the first discrete conduction band level of the quantum dot. When $E_{F,tip}$ is raised further and reaches the next level, tunneling through this level can also take place. At a bias such that $E_{F,tip}<E_{F,sub}$ an electron can tunnel from the substrate to tip, via the levels of the valence band. In the current-bias plot a zero current range around ΔE=0 will be found, corresponding to the bandgap of the quantum dot. Steps in the current-bias (*I*-*V*) plot or peaks in the conductance-bias plot (*dI/dV*-*V*) will appear at bias values corresponding to resonant tunneling through discrete

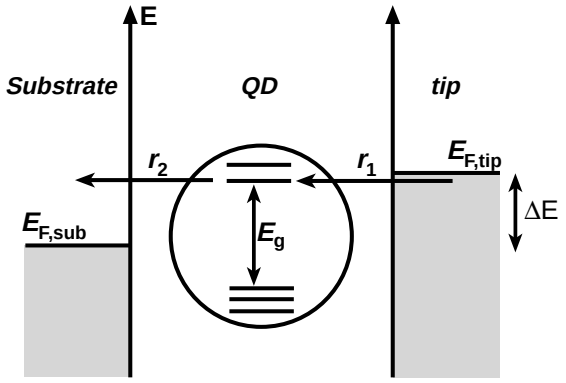

Figure 1.7 *A schematic representation of a DBTJ for a metal/dot/tip configuration. Resonant tunneling via a discrete energy level in the quantum dot can occur when* $E_{F,tip}$ *reaches that level.*

energy levels of the quantum dot. For an unambiguous assignment of the peaks in the *dI/dV* vs *V* curve, it is necessary to have an asymmetrical DBTJ, such that $E_{F,sub}$ is locked to the energy levels of the quantum dot. Furthermore, Tunneling Spectroscopy using an electrostatic gate electrode or a magnetic field can be very helpful in elucidating the electronic structure of semiconducting quantum dots.[68,69]

1.4 Intensity-Modulated Photocurrent Spectroscopy

Intensity-Modulated Photocurrent Spectroscopy (IMPS) is a time-resolved optoelectrical method. In this work the technique is used in a photoelectrochemical context to determine the rate constants of electron tunneling processes between the semiconductor quantum dots and a metal or redox system in the solution. IMPS has previously been used to study recombination processes, majority carrier injection at the bulk semiconductor/electrolyte interface[70], and charge transport in nanoporous semiconductor electrodes.[71-73] In this section the principle of the technique will be briefly described.

In IMPS, a small sinusoidal modulation, $\Phi(\omega)$, is superimposed on a steady-state light intensity, Φ, giving a photocurrent which also has a sinusoidal contribution (ω is the modulation frequency). The modulated photocurrent $j(\omega)$ is measured using frequencies, ω, lower than $(RC)^{-1}$. The ratio $j(\omega)/e\Phi(\omega)$ is called the optoelectrical transfer function. Slow processes contributing to the total photocurrent will lead to a phase shift, $\theta(\omega)$, between $\Phi(\omega)$ and $j(\omega)$. The transfer function, determined by the amplitude ratio and the phase shift, can be plotted in the complex plane (imaginary component vs real component) or in a Bode plot (imaginary or real component vs frequency). In the experimental set-up used here, consisting of an illuminated metal/QD working electrode, the frequencies at which the imaginary part of the function shows

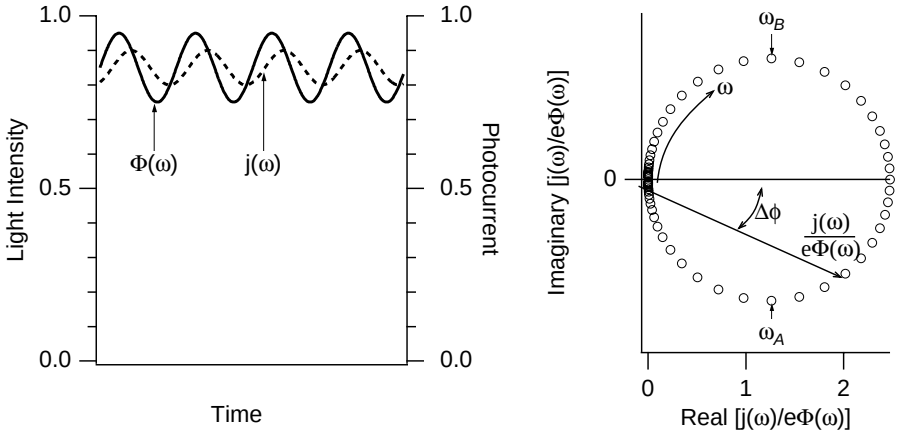

Figure 1.8 *The principle of IMPS. (a) Modulated light intensity and photocurrent as a function of time. The modulation depth is ~10% of the base light intensity. (b) Complex plane plot of the recombination process of a photoexcited state in a semiconductor quantum dot adsorbed on a metal electrode via the metal.* ω_A *and* ω_B *correspond to the rate constants of the anodic and cathodic electron tunneling processes, respectively.*

an extremum correspond to the rate constants of the photoinduced electron transfer between the QD and the metal, or the redox species in the electrolyte. The experimental data and the theoretical derivation of $j(\omega)/e\Phi(\omega)$ are the subject of chapters 2, 3, and 4. In Figure 1.8 the optoelectrical transfer function, which might be expected for the decay of a photoexcited state in the quantum dot via the metal, is shown in the complex plane with the frequency as a parameter. In the high frequency limit electron transfer is slower than the light modulation, and both the real and imaginary components are zero. When the frequency is decreased, the phase shift between $\Phi(\omega)$ and $j(\omega)$ decreases, and a signal is observed. The frequency at the minimum of this semicircle, ω_A, corresponds to the rate constant for electron tunneling from the dot to the gold, since the real component is anodic. When the frequency is further decreased a semicircle in the positive-positive quadrant is observed. The frequency at the maximum of this semicircle, ω_B, corresponds to electron tunneling from the gold to the unoccupied level in the dot. In the low frequency limit the function is zero, meaning that both transfer from the QD to the metal and from the metal to the QD can follow the light modulation.

1.5 Outline of this Thesis

In this thesis a study of resonant electron tunneling between II-VI semiconductor quantum dots and a metal substrate is described. Gold electrodes were provided with a monolayer of quantum dots for the photoelectrochemical measurements and for the STS. Chapters 2, 3 and 4

deal with the study of photoinduced electron tunneling between nanocrystalline CdS, PbS and CdSe particles, respectively, and the gold electrode. In the literature, a long-lived excited state was reported for Q-CdS and Q-CdSe; the exact nature of these states could not be elucidated by optical spectroscopy. The electronic structure of the long-lived excited state in CdS, PbS and CdSe quantum dots was studied with photoelectrochemistry. The resulting picture of the long-lived excited state, complements the data obtained with optical spectroscopy. In CdS and CdSe, the long-lived excited state consists of a hole in a deep trap in the bandgap and an electron in the LUMO, whereas in PbS the electron is deeply trapped and the hole is in the HOMO. These long-lived excited states have a much lower energy than the primary (LUMO-HOMO) exciton. Recombination of the excited state via the gold levels due to consecutive electron tunneling to and from the gold was observed. Steady-state anodic and cathodic photocurrents, due to electron injection from tartrate and electron scavenging by ferricyanide, were also seen.

With IMPS the rate constants of the electron transfer processes were obtained. We found that electron tunneling from the dot to the gold was the fastest process in the CdS/Au and CdSe/Au systems. In the PbS/Au system, electron tunneling from the gold to the unoccupied level in the dot was the fastest process. By varying the temperature, the tunneling processes could be distinguished from a possible electrochemical step; the rate constant of tunneling is, in principle, independent of the temperature, in contrast to that of an electrochemical reaction. A mathematical model was derived and fitted to the experimental results. Experiment and theory were in good agreement. These results indicated that the non-trapped charge carrier has a higher tunnel probability than the trapped charge carrier, which was not completely understood.

In chapter 4, results are described for colloidal CdSe particles, covalently bound to Self-Assembled Monolayers of (non-rigid) dithiols and rigid disulfide spacer molecules. The aim of this work was to study the distance dependence of electron tunneling in the Au/SAM/Q-CdSe assembly. An advantage of such a system is that the photoinduced electron transfer is not thermally activated. Generally, thermally activated electron transfer (ET) forms a serious problem in the interpretation of the distance-dependence of ET, because in most systems the molecular and environmental properties, and hence the reaction free energy, and the activation energy also change with the distance between the electron donor and acceptor. When alkane dithiols were used as spacer molecules, the measured rate constants depended on the applied potential and did not show a trend upon a chain length variation. Probably the SAM deformed on applying a potential and the tunneling distance changes. Possibly due to the flexibility of the molecules, the distance between the dots on the monolayer and the gold was not constant. With a rigid disulfide as a linker between the gold surface and the CdSe dots, the tunneling rate constants depended

exponentially on the distance. A value of 0.5 $Å^{-1}$ was found for β, the decay parameter; this value was rather small in comparison to values found in metal/vacuum/metal systems. Very likely, the wave function in the CdSe quantum dot is coupled to the gold wave functions via a through-bond interaction, in which the σ-orbitals of the cyclohexylidenes and the π-orbitals of the double bonds of the spacer molecules are involved. Photoelectron spectroscopy has shown that the lone pair π–type orbitals of the sulfide groups had a strong interaction in this type of molecule.

In the work described in chapter 5, resonant tunneling in a Au/QD/tip DBTJ was studied using CdS and CdSe quantum dots. With nanocrystals bound to gold via a spacer molecule, the potential was distributed over both junctions of the metal/dot/tip system. In this case, resonant tunneling occured via the levels of the conduction band at positive and at negative bias; the tunneling spectra were quite symmetrical. Quantum dots, electrodeposited epitaxially, were strongly coupled to the gold. An asymmetrical DBTJ was formed when the tip is placed above the dot. In this configuration the substrate Fermi-level was fixed with respect to the energy levels in the dot. When the bias was sufficiently positive or negative, the discrete energy levels of the conduction and valence band were observed, respectively. The potential range of zero current was independent of the dot/tip distance and corresponded to the bandgap of the quantum dot.

An STS study at cryogenic temperatures on the electronic structure of individual CdSe quantum dots is presented in chapter 6. Colloidal CdSe nanoparticles were attached to a bare gold surface. The symmetry of the DBTJ was varied by changing the tip/dot distance and, as a consequence, not only the ratio of capacitances was changed but also the ratio of the rates of electron tunneling to and from the dot. If tunneling from the dot to the substrate was much faster than tunneling from the tip to the dot, the probability that an orbital of the dot was occupied by an electron was very small, and electron-electron Coulomb charging effects were negligible. In this case the conduction and valence band levels were probed, but the degeneracy of the levels was not resolved. If the rates of electron tunneling to and from the dot were comparable, the occupation probability of an orbital in the dot by an electron might be sufficiently high to observe Coulomb charging. Due to the charging, degenerate energy levels could be resolved. The measured electronic structure of CdSe quantum dots could be described on the basis of the model for an electron in a cubic box.

References

1 S.V. Gaponenko, *Optical Properties of Semiconductor Nanocrystals* **1998**, Cambridge University Press, United States of America

2 MRS Bulletin, february **1998**

3 G. Jaeckel, *Z. Tech. Phys.* **1926,** *6***,** 301

4 A. Henglein, *J. Phys. Chem.* **1982**, *86*, 2291-2293

5 L.E. Brus, *J. Chem. Phys.* **1984**, *80*, 4403

6 H. Mattoussi, L.H. Radzilowski, B.O. Dabbousi, D.E Fogg, R.R. Schrock, E.L. Thomas, M.F. Rubner, and M.G. Bawendi, *J. Appl. Phys.* **1999**, *86*, 4390

7 Y. Yang, S. Xue, S. Liu, J. Huang, and J. Shen, *Appl. Phys. Lett.* **1996**, *69*, 377

8 D.L. KLein, P.L. McEuen, J.E. Bowen Katari, R. Roth, and A.P. Alivisatos, *Appl. Phys. Lett.* **1996**, *68*, 2574

9 M.A. Kastner, *Nature* **1997**, *389*, 667

10 D.L. KLein, R. Roth, A.K.L. Lim, A.P. Alivisatos, and P.L. McEuen, *Nature* **1997**, *389*, 699

11 H. Weller, *Advanced Materials* **1993**, *5*, 88

12 J. Fang, J. Wu, X. Lu, Y. Shen, and Z. Lu, *Chem. Phys. Lett.* **1997**, *270*, 145

13 S. Kohtani, A. Kudo, and T. Sakata, *Chem. Phys. Lett.* **1993**, *206*, 166

14 C. Nasr, P.V. Kamat, and S. Hotchandani, *J. Electroanal. Chem*. **1997**, *420*, 201

15 D. Liu, and P.V. Kamat, *J. Phys. Chem.* **1993**, *97*, 10769

16 Y.A. Vlasov, N. Yao, and D.J. Norris, *Advanced Materials* **1999**, *11*, 165

17 V.L. Colvin, M.C. Schlamp, and A.P. Alivisatos, *Nature* **1994**, *370*, 354

18 B.O. Dabbousi, M.G. Bawendi, O. Onitsuka, and M.F. Rubnar, *Appl. Phys. Lett.* **1995**, *66*, 1316

19 A.P. Alivisatos, K.P. Johnsson, X. Peng, T.E. Wilson, C.J. Loweth, M.P. Bruchez jr, and P.G. Schultz, *Nature* **1996**, *382*, 609

20 D.F. Ollis, H. Al-Ekabi, Photocatalytic Purification and Treatment of Water and Air, Elsevier Science Publishers **1993**, Amsterdam, The Netherlands

21 C. Dekker, *Physics. Today* **1999**, *52*, 22

22 J.R. Arthur, *J. Appl. Phys.* **1968**, *39*, 4032

23 A.Y. Cho, *J. Vac. Sci. Technol.* **1971**, *8*, S31

24 D. Heitmann, and J P. Kotthaus, *Physics Today* **1993**, *june*, 56

25 M.A. Kastner, *Physics Today* **1993**, *january*, 24

26 U. Rothlisberger, W. Andreoni, M. Parinello, *Phys. Rev. Lett.* **1994**, *72*, 665

27 L. Spanhel, M. Haase, H. Weller, and A. Henglein, *J. Am. Chem. Soc.* **1987**, *109*, 5649

28 M.L. Steigerwald, A.P Alivisatos, J.M. Gibson, T.D. Harris, R. Kortan, A.J. Muller, A.M. Thayer, T.M. Duncan, D.C. Douglas, L.E. Brus, *J. Am. Chem. Soc.* **1988**, *110*, 30460

29 X. Peng, L. Manna, W. Yang, J. Wickham, E. Scher, A. Kadavanich, and A.P. Alivistatos, *Nature* **2000**, *404*, 59-61

30 C.B. Murray, D.J. Norris, and M.G. Bawendi, *J. Am. Chem. Soc* **1993**, *115*, 8706

31 H. Matsumoto, T. Sakata, H. Mori, H. Yoneyama, *J. Phys. Chem. B* **1996**, *100*, 13781

32 A. van Dijken, A. Meijerink, D. Vanmaekelbergh, *Chem. Phys. Lett.* **1997**, *269*, 494

33 N.W. Ashcroft, and N.D. Mermin, *Solid State Physics* **1976**, Philadelphia

34 L.E. Brus, *J. Phys. Chem.* **1986**, *90*, 2555

35 P.W. Atkins, *Physical Chemistry* **1990**, Oxford University Press, Great Brittain

36 H.M. Schmidt, and H. Weller, *Chem. Phys. Lett.* **1986**, *129*, 615-618

37 A. Henglein, *Topics in Current Chemistry* **1988**, *143*, 115

38 A.P. Alivisatos, *J. Phys. Chem.* **1996**, *100*, 13226

39 A.J. Nozik, and O.I. Micic, *MRS Bulletin* february **1998**, 24

40 M. Kuno, J.K. Lee, B.O Dabbousi, F.V. Mikulec, and M.G. Bawendi, *J. Chem. Phys.* **1997**, *106*, 9869

41 M.T. Nenadovic, M.I. Comor, V. Vasic, and O.I. Micic, *J. Phys. Chem.* **1990**, *94*, 6390

42 P. Guyot-Sionnest, and M.A. Hines, *Appl. Phys. Lett.* **1998**, *72*, 686

43 W.J. Albery, G.T. Brown, J.R. Darwent, and E. Saievar-Iranizad, *J. Chem. Soc. Faraday Trans. 1* **1985**, *81*, 1999

44 R. Wiesendanger, *Scanning Probe Microscpoy and Spectroscopy* **1994**, Cambridge University Press, Great Britain

45 G. Binnig, H. Rohrer, Ch. Gerber, and E. Weibel, *Phys. Rev. Lett.* **1982**, 49, 57

46 J.E. Lilienfeld, *Z. Phys.* **1922**, *23*, 506

47 E.W. Müller, *Z. Phys.* **1937**, *106*, 541

48 J. Bardeen, *Phys. Rev. Lett.* **1961**, *6*, 57

49 P.V. Gray, *Phys. Rev.* **1965**, *140*, A179

50 V.L. Colvin, A.N. Goldstein, and A.P. Alivisatos, *J. Am. Chem. Soc.* **1992**, *114*, 5221

51 J.E. Bowen Katari, V.L.Colvin, and A.P. Alivisatos, *J. Phys. Chem.* **1994**, *98*, 4109

52 S. Ogawa, F.F. Fan, and A.J. Bard, *J. Phys. Chem. B* **1995**, *99*, 11182

53 S. Ogawa, K. Hu, F.F. Fan, and A.J. Bard, *J. Phys. Chem. B* **1997**, *101*, 5707

54 M. Miyaki, H. Matsumoto, M. Nishizawa, T. Sakata, H. Mori, S. Kuwabata, and H. Yoneyama, *Langmuir* **1997**, 13, 742

55 S. Drouard, S.G. Hickey, and D.J. Riley, *Chem. Commun.* **1999**, *8*, 67

56 T. Nakanishi, B. Ohtani, K. Uosaki, *J. Phys. Chem .B* **1998**, *102*, 1571

57 G. Hodes, I.D.J. Howell, and L.M. Peter, *J. Electrochem. Soc.* **1992**, *139*, 3136

58 B. Alperson, H. Demange, I. Rubinstein, and G. Hodes, *J. Phys. Chem. B* **1999**, *103*, 4943

59 Y. Golan, G. Hodes, and I. Rubinstein, *J. Phys. Chem.* **1996**, *100*, 2220

60 Y. Kuk, M.F. Jarrold, P.J. Silverman, J.E. Bower, and W.L. Brown, *Phys. Rev. B* **1989**, *39*, 11168

61 R.H.M. Groeneveld, M.W.J. Prins, and H. van Kempen, *Surface Science* **1995**, *331-333*, 1299

62 B. Alperson, S. Cohen, I. Rubinstein, and G. Hodes, *Phys. Rev. B.* **1995**, *52*, R17017

63 T.D. Krauss, and L.E. Brus, *Phys. Rev. Lett.* **1999**, *83*, 4840

64 P.J.M. van Bentum, R.T.M. Smokers, and H van Kempen, *Phys. Rev. Lett.* **1988**, *60*, 2543

65 R.P. Andres, T Bein, M. Dorogi, S. Feng, J.I. Henderson, C.F. Kubiak, W. Mahoney, R.G. Osifchin, and R. Reifenberger, *Science* **1996**, *272*, 1323

66 C. Schönenberger, H van Houten, H.C. Donkersloot, A.M.T. van Putten, and L.G.J. Fokkink, *Physica Scripta* **1992**, *T45*, 289

67 U. Banin, Y.W. Cao, D. Katz, and O. Millo, *Nature* **2000**, *400*, 542-544

68 L. Gurevich, L. Canali, and L.P. Kouwenhoven, *Appl. Phys. Lett.* **2000**, *76*, 384-386

69 D.C. Ralph, C.T. Black, and M. Tinkham, *Phys. Rev. Lett.* **1997**, *78*, 4087-4090

70 D. Vanmaekelbergh, A.R. de Wit, and F. Cardon, *J. Appl. Phys.* **1993**, *73*, 5049

71 P.E. de Jongh, and D. Vanmaekelbergh, *Phys. Rev. Lett.* **1996**, *77*, 3427

72 D. Vanmaekelbergh, F. Iranzo Marin, and J. van de Lagemaat, *Ber. Bunsenges. Phys. Chem.* **1996**, *100*, 616

73 L.M. Peter, and D. Vanmaekelbergh, *'Advances in Electrochemical Science and Engineering'* **1999**, John Wiley & Sons, Weinheim, Germany, 77